Earth and Planetary Science Letters 437 (2016) 127–137

Contents lists available at ScienceDirect

Earth and Planetary Science Letters

www.elsevier.com/locate/epsl

The provenance of Taklamakan desert sand

Martin Rittner [a,*], Pieter Vermeesch [a], Andrew Carter [a,b], Anna Bird [c], Thomas Stevens [d], Eduardo Garzanti [e], Sergio Andò [e], Giovanni Vezzoli [e], Ripul Dutt [f], Zhiwei Xu [g], Huayu Lu [g]

[a] London Geochronology Centre, Department of Earth Sciences, University College London (UCL), London, WC1E 6BT, UK
[b] Department of Earth and Planetary Sciences, Birkbeck College, University of London, London, WC1E 7HX, UK
[c] Department of Geography, Environment and Earth Sciences, University of Hull, Cottingham Road, Hull, HU6 7RX, UK
[d] Department of Earth Sciences, Uppsala Universitet, Villavägen 16, 752 36 Uppsala, Sweden
[e] Department of Earth and Environmental Sciences, Università di Milano-Bicocca, Piazza della Scienza 4, 20126 Milano, Italy
[f] Indian Institute of Technology, Roorkee, Uttarakhand, 247667, India
[g] School of Geographic and Oceanographic Sciences, Institute for Climate and Global Change Research, Nanjing University, Nanjing 210093, China

ARTICLE INFO

Article history:
Received 11 May 2015
Received in revised form 24 December 2015
Accepted 27 December 2015
Available online 15 January 2016
Editor: A. Yin

Keywords:
Tarim
multi-proxy
provenance analysis
MDS mapping
Chinese Loess Plateau

ABSTRACT

Sand migration in the vast Taklamakan desert within the Tarim Basin (Xinjiang Uyghur Autonomous region, PR China) is governed by two competing transport agents: wind and water, which work in diametrically opposed directions. Net aeolian transport is from northeast to south, while fluvial transport occurs from the south to the north and then west to east at the northern rim, due to a gradual northward slope of the underlying topography. We here present the first comprehensive provenance study of Taklamakan desert sand with the aim to characterise the interplay of these two transport mechanisms and their roles in the formation of the sand sea, and to consider the potential of the Tarim Basin as a contributing source to the Chinese Loess Plateau (CLP). Our dataset comprises 39 aeolian and fluvial samples, which were characterised by detrital-zircon U–Pb geochronology, heavy-mineral, and bulk-petrography analyses. Although the inter-sample differences of all three datasets are subtle, a multivariate statistical analysis using multidimensional scaling (MDS) clearly shows that Tarim desert sand is most similar in composition to rivers draining the Kunlun Shan (south) and the Pamirs (west), and is distinctly different from sediment sources in the Tian Shan (north). A small set of samples from the Junggar Basin (north of the Tian Shan) yields different detrital compositions and age spectra than anywhere in the Tarim Basin, indicating that aeolian sediment exchange between the two basins is minimal. Although river transport dominates delivery of sand into the Tarim Basin, wind remobilises and reworks the sediment in the central sand sea. Characteristic signatures of main rivers can be traced from entrance into the basin to the terminus of the Tarim River, and those crossing the desert from the south to north can seasonally bypass sediment through the sand sea. Smaller ephemeral rivers from the Kunlun Shan end in the desert and discharge their sediment there. Both river run-off and wind intensity are strongly seasonal, their respective transport strength and opposing directions maintain the Taklamakan in its position and topography.

1. Introduction

The Taklamakan is the largest desert in China and one of the largest sand seas in the world, second only to the Rub' al-Khali in Arabia. At an altitude of >1000 m, it occupies the central part of the internally drained Tarim Basin. This basin is surrounded by some of the world's highest mountain ranges, including the Kunlun Shan and Altun Shan (south), Tian Shan (north) and Pamir (west), which are the latest expressions in a succession of tectonic events that have shed sediments of regionally varying thickness up to ~15 km (Kao et al., 2001) onto the continental Tarim Block since the Jurassic (Sobel, 1999). The Taklamakan itself may have formed as early as 26.7–22.6 Ma (Zheng et al., 2015) and is currently a major source of fine grained dust (<2–3 μm) in East Asia that influences both the regional and global climate through scattering of solar radiation and changing cloud properties (Huang et al., 2014). Taklamakan dust storm events are known to have global reach, delivering dust to the Pacific Ocean, North America, Greenland and the Atlantic Ocean (Svensson et al., 2000; Yumimoto et al., 2009). Some of this dust may be carried across the Hexi Corridor to the

* Corresponding author.
E-mail address: m.rittner@ucl.ac.uk (M. Rittner).

http://dx.doi.org/10.1016/j.epsl.2015.12.036

Loess Plateau region and southeastern China (e.g. Liu et al., 2011; Yumimoto et al., 2009), although the role of the Taklamakan as a source of loess-forming dust in the past and the present-day is controversial (Sun, 2002; Bird et al., 2015). Despite this significance as a globally important dust source, the nature of the sand sources to the Taklamakan itself has not been explored in detail. Some bulk geochemical data from Taklamakan dune sand from the eastern part of the basin have been published (Chen et al., 2007; Yang et al., 2007; Xu et al., 2011), as well as a single detrital zircon U–Pb age data set (Xie et al., 2007), but the precise source regions of the desert sand and their spatial heterogeneity are not known. This is of special interest in light of recent detrital zircon U–Pb dating of desert sands from the Mu Us desert in central northern China, that showed stark spatial heterogeneity in sand source (Stevens et al., 2013). Without proper characterisation of the sand sources to the desert itself, its role and impact as a past dust source remains unclear.

The origin of the word 'Taklamakan' has been lost over time, but according to popular tradition, it means "he who goes in shall never come out". It is because of this inaccessibility that the interior parts of the desert remained unexplored until petroleum was found in the 1990s, and two desert-crossing highways were constructed (Dong et al., 2000). Taking advantage of these new access points, we here present a comprehensive provenance study of this desert, using a combination of multiple provenance proxies and state-of-the art statistical analysis.

There is an ongoing debate in sedimentology and in Quaternary paleoclimatology about the production of desert sands and silt in arid and semi-arid regions. In summary, the main views on desert sand generation are either fresh sediments being delivered from surrounding areas and "maturing" in the desert area, or alternatively, potentially multi-phase, in-place recycling of older sediments derived from in-situ weathering of bedrock and/or sedimentation during a different climatic phase. For the generation of loess, it is debated whether the bulk of the silt-sized quartz fraction is delivered by glacial processes, aeolian abrasion on sand dunes, or weathering (Knippertz and Stuut, 2014; Amit et al., 2014; Crouvi et al., 2010; Smith et al., 2002). The role of fluvial transport interaction with arid sandy areas is also an active field of research (e.g. Bullard and McTainsh, 2003; Stevens et al., 2013; Field et al., 2009). Whatever the mechanism of sediment generation and transport, for large aeolian dune fields to continue to exist, there must be a steady supply of transportable material, and yet in many cases, the sediment pathways and sources are not well known.

At the outset of this study, we may consider two competing sand transport mechanisms: wind and water. Current Resultant Drift Potential for sand transport by wind is from the north to the south (Wang et al., 2002). According to geological evidence from up to >1500 m thick Pliocene deposits including windblown sands along the southern margin of the Tarim Basin, these conditions have persisted since at least 5.3 Ma (Sun and Liu, 2006) and possibly the late Oligocene (Zheng et al., 2015). However, the main rivers flow in the opposite direction, from south to north and then east, aided by a gentle slope from elevations of ca. 1500 m in the south of the basin to ca. 900 m in the north and east (Fig. 1). Most of these rivers are ephemeral, only the Hotan He and the Yarkan He cross the desert year long, though fluvio-lacustrine sediments in the dune valleys across large parts of the desert testify to floods and water flow occurring during the snow melt in June–August. Given the current prevalent wind directions and thick stratigraphic successions preserved along the southern margin, it might appear that a large part of the sand must be blown from the north, derived from the fluvial fans coming off the Tian Shan, or even transported over long distances from Central Asian sources including the Junggar Basin. Yet, it may equally be argued that the northward flowing rivers, following topographic gradient, could achieve a constantly large supply of sediment outweighing basin subsidence. So far, few studies have considered the interplay of fluvial and aeolian sediment transport in a comparable setting to the study area (e.g. Field et al., 2009; Bullard and McTainsh, 2003).

To gain a more complete understanding of sand transport in the Tarim Basin, we collected a large multivariate provenance dataset based on detrital-zircon geochronology (dZ), heavy-mineral (HM) and bulk-petrography (PT) analyses of 39 sand samples from the main tributaries and representative alluvial fans feeding into the Tarim Basin, and from Taklamakan dunes. The dataset includes several samples from the Junggar Basin and the southern Altai for comparison, to test whether these areas may have been a source of sediment carried by winds from this basin into the Tarim area (Fig. 1). A previous small-scale study across the central Tarim Basin, based on visual comparison of whole-rock geochemical data from samples collected along the eastern desert-crossing highway and from the Keriya River (Yang et al., 2007), suggested that it should be possible to discriminate local source areas due to a low degree of E–W mixing. In order to recognise sediment pathways, our more detailed study required the interpretation of large multiple proxy datasets, so we used an established statistical method known as multidimensional scaling (MDS) that has been adopted for provenance studies (Vermeesch, 2013; Stevens et al., 2013; Vermeesch and Garzanti, 2015). This provides an efficient, unbiased way to visualise relations within multi-sample datasets, and greatly helps to subsequently interpret the full data set in detail.

2. Regional overview

The Tarim Basin (Fig. 1) covers an area of over 600 000 km^2 and stretches some 1100 km E–W and 600 km N–S. The basin is fringed by tectonically active mountain ranges: the Tian Shan to the north and the Kunlun and Altun Mountains (Altyn Tagh) to the south. The central parts of the basin contain the active sand desert that covers more than half of the total area of the basin (330 000 km^2). Atmospheric circulation is dominated by a high-pressure centre which sits above the northwestern part of the desert and produces winds that blow from the north in the northern part of the desert and from the east in the central and southern parts (Fig. 1). Thus, net aeolian sand transport is in a south-westerly direction (Dong et al., 2000; Wang et al., 2002), which generally coincides with the orientation of larger dune features (Tsuchiya and Oguro, 2007), including large-scale (1–2.5 km wide and 50–200 m high) linear sand dunes, large (100 s of m high) star dunes (Tsuchiya and Oguro, 2007), and areas of complex, smaller-scale compound dunes (Wang et al., 2002). Mean annual precipitation decreases from 100 mm in the northeast to 50 mm in the central region.

The main Tarim river originates at the confluence of the Yarkan and the Kashgar Rivers, draining the eastern Pamir and westernmost Kunlun Mountains, respectively, and flows eastward around the northern edge of the Taklamakan desert (Fig. 1). 60–80% of its annual run-off is confined to the flood season between June and August. During this period, the river carries more than 80% of its annual sediment load (Ye et al., 2014), and for most of the remaining months, river levels are low, allowing the flood plains to dry out and potentially be remobilised by wind erosion. As the Tarim River is dependent on glacial melt waters for ca. 48% of annual run-off (Chen et al., 2006), tributaries with glaciated catchments are important sources of sediment. The Tarim River receives water from three rivers that have catchments in glaciated mountains: the Hotan drains the Kunlun, the Yarkan the Karakorum, Pamir and Kunlun, and the Aksu (including Toshkan) the Tian Shan. The Aksu drains the most heavily glaciated part of the Tian Shan and thus,

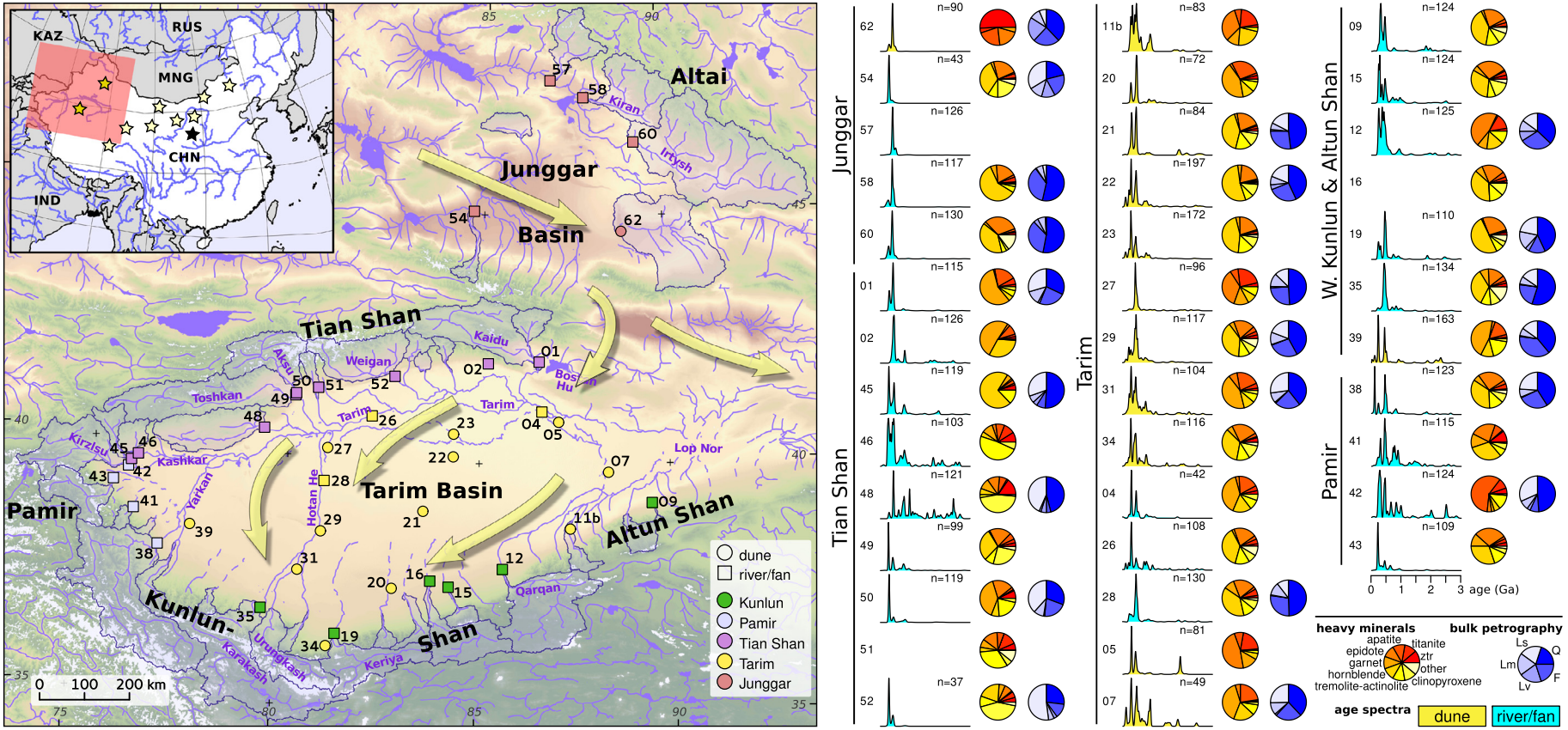

Fig. 1. Left: sampling locations. Base map SRTM data (Jarvis et al., 2008). Prevailing wind directions indicated in yellow, modified after Sun and Liu (2006) and Yumimoto et al. (2009). Drainage network and sampled catchment areas calculated from DEM, indicated in blue. Inset: Stars indicate location of potential source areas (yellow: this study, pale yellow: other areas) of the Chinese Loess Plateau (black star) discussed in Stevens et al. (2013). Right: adaptive kernel density estimates, bulk sediment and heavy mineral compositions. The U–Pb age distributions are using a common bandwidth of 25 Ma. Distinction is made between fluvial (blue) and aeolian samples (yellow). Numbers indicate sample locations. Q – quartz, F – feldspar, Lm – metamorphic lithics, Lv – volcanic lithics, Ls – sedimentary lithics, ztr – zircon, tourmaline and rutile. (For interpretation of the references to colour in this figure legend, the reader is referred to the web version of this article.)

although its drainage area constitutes only 5% of the entire Tarim catchment, its average annual water flow accounts for 70–80% of the annual flow of the Tarim River (Kundzewicz et al., 2015). As a consequence, the Aksu River drainage basin delivers a significant amount of sediment to the Tarim River, some of which could be remobilised from the flood plains further east.

Most of the smaller river beds draining the Kunlun and Altun Shan end at the foot of the alluvial fans, where those border the sandy desert in the south. In the flood season, the streams may reach far into the desert and contribute to flooding of dune valleys and northward sand transport, whereas in the dry season, some rivers completely dry out.

The zircon U–Pb age signatures, heavy-mineral, and bulk-petrography characteristics of the sampled sands are defined by the geological evolution of the Tarim Basin and the different histories of crustal growth in each mountain range surrounding the basin. This history dates back to several small Archaean terranes, that by amalgamation during the early to middle Neoproterozoic formed the Tarim Craton (Zhang et al., 2013). Exposed basement, found mainly along the northern and eastern margins of the basin, includes 2.80–2.57 Ga granitoid gneisses, 2.1–1.8 Ga arc-related assemblages associated with the Columbia supercontinent, 1.0–0.9 Ga alkaline volcanics, metasediments and metavolcanics linked to the assembly of the Rodinia supercontinent (Zhang et al., 2013; Ge et al., 2014), and 820–760 Ma igneous units linked to subsequent breakup of Rodinia (Shu et al., 2011; Xu et al., 2005; Zhang et al., 2009). The geology of the mountains that surround the Tarim Craton resulted from a protracted succession of Paleozoic–Mesozoic collisions between mainly Proterozoic continental fragments and younger island arcs that accreted to Asia (Xiao et al., 2005, 2013; Yang, 2002).

The Western Kunlun formed by progressive closure of the paleo-Tethyan ocean when the southern Tarim was an active continental margin (Yin and Harrison, 2000; Cowgill et al., 2003). Magmatism and accretionary events started from 470–400 Ma and 350–220 Ma, and ended with emplacement of small, ca. 214 Ma (Late Triassic) granitoids at the end of the Andean-type Cimmerian orogenesis (Xiao et al., 2005). By contrast, in the section of the Kunlun adjacent to the Altun Shan, plutons and volcanic rocks of arc affinity were formed between 370–320 Ma and 270–210 Ma (Dai et al., 2013). Final closure and collision between the southern Tarim active margin and the Qiangtang block occurred in the Late Jurassic (Roger, 2003). The Tian Shan resulted from accretion of island arcs and microcontinents between the Early Paleozoic and the Permian–Early Triassic, including Carboniferous amalgamation between the Yili (Kazakhstan) and Tarim blocks (Zhang et al., 2013). Typical zircon ages for subduction-related and post-collisional granitoids cluster between 480–390 Ma and 320–270 Ma (Xiao et al., 2013). Most of these former collision zones were reactivated and uplifted in the Cenozoic (Carroll et al., 2013) in response to far-field strain resulting from the India–Asia collision (Dumitru et al., 2001).

Whilst sedimentation on the Tarim Block began during the Paleozoic accretion events, key periods of subsidence of today's Tarim Basin took place in: a) the Cenozoic, linked to the collision between India and Asia which caused further loading through the overthrusting of the Tarim Basin margins by the Tian Shan in the north (Allen et al., 1999), by the Pamir in the west (Coutand et al., 2002; Cowgill, 2010), and by the Kunlun Shan–Altun Shan in the south (Jiang, 2004), and b) the Late Cretaceous, when flexural loading produced two foreland basins along the southern margin of the nascent Tian Shan and the northeastern margin of the West Kunlun Shan (Yang, 2002). Between the Cenomanian and the Early Oligocene, subsidence was accompanied by five major marine incursions linked to Paratethys, although connections to Paratethys may have continued until the Middle Miocene (Bosboom et al., 2014). The final retreat of the Paratethys Sea from Central Asia as well as uplift of the Tibetan Plateau changed the regional land-sea thermal balance and contributed to the aridification that resulted in formation of the Taklamakan desert (Zhang et al., 2007, 2015).

3. Sampling locations and methodology

The internal drainage system of the Tarim Basin, fed by a mountainous fringe, provides an excellent opportunity to study sediment pathways, to discriminate the roles of water and wind transport, and to understand the extent to which contributing source area signatures are preserved or mixed in this arid environment. The sampling locations (Fig. 1) were chosen so as to cover the Taklamakan and the main catchments and alluvial fans draining the surrounding mountains. Samples from the Junggar Basin were collected for comparison only, without attempt to cover this region comprehensively. Dune samples were taken at the dune crest, in locations upwind away from any anthropogenic features. River sediments were taken from recently deposited, unaltered sand bars, sampled as far as possible across several laminae of internal cross-bedding to reduce hydraulic-sorting bias. A similar strategy was attempted on tributary fans where feasible, by digging into the subsurface and avoiding the blown-out sediment surface. To define provenance signatures, we characterised samples in terms of their bulk petrography (PT), heavy mineral composition (HM), and detrital zircon U–Pb age (dZ) distribution (Fig. 1). A PT sample comprises 400 point counts, a HM sample 200 point counts, and a dZ sample ~150 individual single grain measurements (yielding ~100–120 concordant ages). For detailed methodology, please see supplemental material.

The resulting dataset (39 samples total) comprises 4047 zircon U–Pb ages (37 samples), 14 027 heavy-mineral point counts (38 samples), and 8800 petrographic point counts (22 samples). Individual samples may be visualised as kernel density estimates (KDEs) for the U–Pb data (Vermeesch, 2012) and histograms or pie charts for the heavy mineral and petrographic data (Fig. 1). As a result, Fig. 1 exhibits 92 individual data plots, and requires $666 + 703 + 231$ cross-comparisons for the dZ, HM and PT data respectively. Given such a large and multivariate dataset, it becomes difficult to properly interpret the raw measurements and relationships by visual inspection alone, so we applied several layers of statistical simplification to extract meaningful information. Firstly, we quantified the pairwise distances between samples as scalars. This was done with the Kolmogorov–Smirnov statistic (for the U–Pb data), the Bray–Curtis distance (for the heavy-mineral data), and Aitchison's central logratio distance (for the bulk petrography; Vermeesch and Garzanti, 2015). This produced three pairwise distance tables that were then each fed into a multidimensional scaling (MDS) algorithm.

MDS is a dimension-reducing technique that aims to visualise the data as a 'map' preserving differences between samples as relative distances between the data (Vermeesch, 2013), and has been successfully applied to e.g. desert sand data of the Mu Us desert in north central China (Stevens et al., 2013). For the present study, three such maps were produced, one for each dataset (see supplementary material). For the dZ and HM dataset, we employed a 'non-metric' MDS algorithm, whereas the PT data were analysed by 'classical MDS' (Vermeesch, 2013). The latter is equivalent to Principal Component Analysis (PCA), in which genetic interpretation can be obtained by jointly visualising the configuration and the 'loadings' as a 'biplot' (Fig. 3b, see section 4.6). To further simplify the interpretation, multiple datasets can also be combined into a '3-way MDS analysis' (also known as Individual Differences Scaling or INDSCAL; Vermeesch and Garzanti, 2015). This includes a set of 'weights' for each dataset, which quantify the degree of 'stretching'

that needs to be applied to the horizontal and vertical axis of the 'group configuration' to maximise the fit to that dataset. The result is a 'consensus view' of the entire dataset across multiple samples and multiple methods (Vermeesch and Garzanti, 2015). INDSCAL provides insight not only into which samples are similar to each other and which are different, but also into the underlying mechanisms for these similarities and differences; see section 4.6.

Due to sampling effects, a small number ($< \sim$80–100) of analyses on one sample might result in an age spectrum that imprecisely estimates the true age distribution, and thus plot position of this sample on the MDS map would shift. Unfortunately, there is no easy way to visualise the magnitude of this variability, although for reasonably large sample sets, the 'stress' value (Vermeesch, 2013) is usually a good measure of robustness (see Shepard plots in supplementary material). Thus, positions of single samples on the MDS maps must not be over-interpreted, but the scatter within one well defined geographical group, like the Tarim basin group in Fig. 3a, can give an estimate of uncertainty. For the same reasons, we do not consider height or height ratios of individual peaks in the age spectra for interpretations in this study, only peak positions, and absence of a peak is not used as a binding argument if that observation cannot be confirmed by other proxies or on several samples.

4. Results

In the following, samples are grouped geographically (see Fig. 1 and Table 1), where not addressed individually by reference to sample number. The "Junggar" group comprises samples from north of the Tian Shan, the "Tian Shan" group derive from south draining rivers and fans from the Tian Shan, the "Kunlun" group are samples from the West Kunlun and Altun Shan at the southern margin of the Tarim Basin, and "Pamir" samples are from the westernmost catchments that receive input from the NE Pamir. The remaining samples come from the central Tarim Basin and are grouped as "Tarim". The latter comprise dune sands as well as samples from rivers within the basin (04, 26, 28). One sample of loess from the foothills of the Kunlun mountains (34), which is considered to represent a natural average of windblown sediments from the Tarim Basin, is also included in this group.

4.1. Kunlun Shan

Sediments of the southern rivers (Qarqan, Keriya and Karakash; 12, 19, 35, respectively) draining the Kunlun Shan are generally feldspatho-litho-quartzose, similar to the Tarim dune sands. The heavy-mineral suites are also similar. However, the grains, especially the softer lithologies, are less well rounded than in the desert sands (see Fig. 4).

In the detrital zircon age spectra, the northwestern Kunlun yields ages from 350 Ma to 220 Ma, while the areas closer to the Altun Shan show two peaks of 370–320 Ma and 270–210 Ma. The Kunlun-derived samples overlap the Tarim Basin sands with a close fit on the MDS maps (Fig. 3 and supplementary material).

Sample 19 (like Tarim sample 31) derives from downstream of the Western Kunlun loess region and shows a high grade of mixing of proxy signatures.

4.2. Pamir

The petrographic compositions of Yarkan River sands (sample 38; Fig. 1) in the southwestern part of the basin are indistinguishable from Tarim dune sands. Both share feldspatho-quartzo-lithic to litho-feldspatho-quartzose compositions and contain the same common sedimentary (limestone, shale, dolostone, siltstone/sandstone) and very low grade to high grade metamorphic rock fragments (metapsammite, metapelite). Heavy mineral suites are also similar, dominated invariably by amphiboles (dominantly blue-green hornblende) with associated epidote-group minerals (dominantly pistacite) and significant amounts of pyroxenes and garnet.

The western rivers (Kirzlsu, 42, and Kashgar resulting from confluence with 43, 45, 46) from the NE Pamir and westernmost Tian Shan carry different litho-quartzose sands with higher quartz/feldspar ratios, more sedimentary to low-grade metasedimentary rock fragments, and poorer heavy mineral assemblages dominated by either epidote or clinopyroxene, indicating an additional volcanic source in the hinterland.

Precambrian zircons are rare or absent in most samples except from the southwestern-most Tian Shan and the Pamir (48, 46, 42, also dune 39). Youngest zircon age groups, $<$120 Ma, are confined to sands of the Yarkan and Kashgar rivers (38, and 41–43) that drain the northeastern Pamir and westernmost Kunlun, and are traceable further downstream along the main Tarim River (26, 7, 22, 23).

4.3. Tian Shan

The Northern rivers (Aqal, Toshkan, Aksu, Weigan and Kaidu; 48, 49, 50, 52, 01, respectively) that drain the Tian Shan carry

Table 1
Sampling locations by geographic region. PT – bulk petrographic data presented. HM – heavy mineral data presented. dZ – detrital zircon U–Pb age data presented.

Sample	Type	Map name	PT	HM	dZ
Tian Shan					
01	river	Kaidu	x	x	x
02	piedmont			x	x
45	river		x	x	x
46	river			x	x
48	river		x	x	x
49	river	Toshkan		x	x
50	river	Aksu	x	x	x
51	piedmont			x	
52	river	Weigan	x	x	x
W. Kunlun and Altun Shan					
09	piedmont			x	x
12	river	Qarqan	x	x	x
15	piedmont			x	x
16	river			x	
19	river	Keriya	x	x	x
35	river	Karakash	x	x	x
Pamir					
38	river	Yarkan	x	x	x
41	stream/fan			x	x
42	river	Kirzlsu	x	x	x
43	piedmont			x	x
Tarim Basin					
04	overbank	Tarim		x	x
05	dune			x	x
07	dune		x	x	x
11b	dune			x	x
20	dune			x	x
21	dune		x	x	x
22	dune		x	x	x
23	dune			x	x
26	overbank	Tarim		x	x
27	dune		x	x	x
28	river	Hotan	x	x	x
29	dune		x	x	x
31	dune		x	x	x
34	loess			x	x
39	dune		x	x	x
Junggar Basin					
54	overbank		x	x	x
57	river			x	x
58	river	Kiran	x	x	x
60	river	Irtysh	x	x	x
62	dune		x	x	x

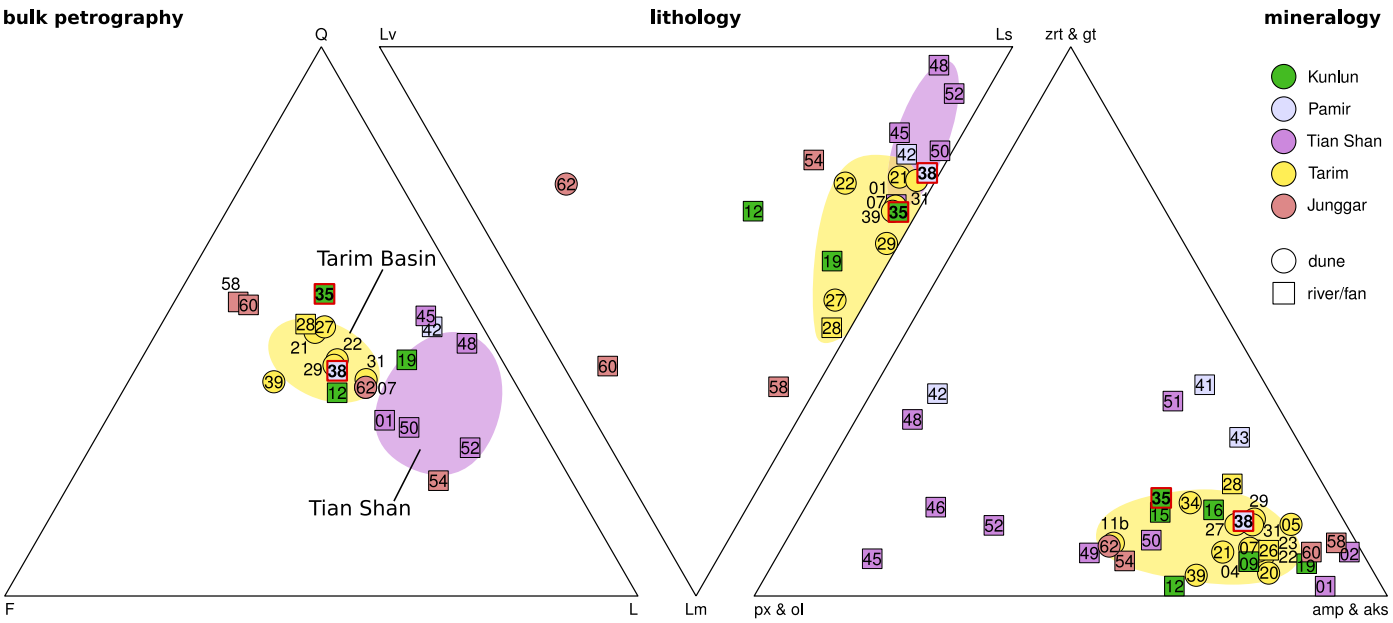

Fig. 2. Sample compositions. QFL highlights framework petrography, whereas Ls–Lv–Lm illuminates the nature of the source areas. ztr&gt–px&ol–amp&aks is chosen as an example of relationships of these indicative minerals. Q – quartz, F – feldspar, L – lithic components, Lv – volcanic lithics, Lm – metamorphic lithics, Ls – sedimentary lithics, ztr – zircon, tourmaline and rutile, gt – garnet, px – pyroxene, ol – olivine, amp – amphibole, aks – andalusite, kyanite and sillimanite. Hotan and Yarkan Rivers (35 and 38, respectively) highlighted.

quartzo-lithic to feldspatho-quartzo-lithic sands dominated by sedimentary to low/medium-grade metasedimentary detritus, reflecting prominent supra-crustal sources distinct from those of Tarim dune sands.

Zircon ages between 315 and 280 Ma derive from Tian Shan late-stage-subduction and post-collision magmatism (Seltmann et al., 2011; Yang et al., 2013).

A strong age peak of ~290–280 Ma in samples coming from the Tian Shan (49, 50, 52) can be found in the Tarim River and nearby dune samples further downstream to the east (26, 04, 05, 07), and in the northeastern dune samples (22, 23, close to an old/seasonal branch of the Tarim itself), but is missing upstream to the west and in the Yarkan. Aksu and Toshkan (50 and 49, respectively) plot amongst the closest data points to the Tarim Basin cluster out of the Tian Shan samples in Figs. 2 and 3.

4.4. Tarim Basin

In the plots in Figs. 2, 3 and supplementary material, the Tarim Basin samples form a very well defined cluster. The Yarkan river (38) and Karakash (/Hotan) river (35) plot on or in direct proximity of the Tarim field, ranking these amongst the likely sources for the basin fill. Whereas the Yarkan shows the exact bulk composition of Tarim Basin sands on the MDS map (supplemental material), it exhibits more sedimentary lithic components on the PCA plot (Fig. 3b), with the Karakash containing a little more quartz. Both have a similar mineralogical composition to the Tarim sands.

Visually, the zircon KDE plots of Tarim Basin river and dune samples appear similar (Fig. 1), dominated by ages between ca. 500 and 200 Ma in a "double peak" pattern: Prominent peaks between 470 and 400 Ma are consistent with sources from the arc and accretionary rocks that form the Tian Shan and Kunlun regions bordering the Tarim Craton (Gehrels et al., 2003, 2011); the second most prominent ages fall between 320 and 210 Ma. As an exception this pattern, the Karakash (sample 35) shows a distinctive age spectrum dominated by only one single 460–400 Ma peak, which is found again downstream along the Hotan He at 29, 28 and all the way north at 27.

The 120 Ma age group from the Yarkan and Pamir is missing in dune sand from the centre and south of the basin (20, 21, 11b, 27, 29), but appears in samples associated with the Tarim River (26, 23, 22, 07).

Sediments from closest to the hydrological sediment sink in the Lop Nor region (sample 07, see map Fig. 1), and a loess and a dune sample from the region where the prevailing winds converge (samples 34 and 31, respectively), show the most diverse age spectra amongst those samples that do not represent single tributary rivers. Dune samples 22 and 23 are situated near past/seasonal trunks of the main Tarim River, and thus also show influence from most source proxy signatures.

4.5. Junggar Basin

In the Junggar Basin, dune sands are feldspatho-quartzo-lithic. Tian-Shan-derived sample 54 is sedimentoclastic with common shale/slate and siltstone/metasilt stone rock fragments, and Altai-derived sample 62 is volcanoclastic, with mainly microlitic volcanic and felsic/in termediate metavolcanic lithics, indicating dominant supra-crustal sedimentary/metasedimentary and volcanic/metavolcanic sources, respectively. These compositions do not match the sands of the Kiran and Irtysh Rivers (58, 60) that drain the southern Altai, which are litho-feldspatho-quartzose metamorphiclastic and rich in micas and heavy minerals.

The Junggar–Altai samples exhibit a much narrower range of zircon ages than the other areas, from 520 to 350 Ma, with one dominant peak at 400 Ma. However, sample 54, fed by a catchment in the Tian Shan, shows a predominant 290 Ma, and a smaller 400 Ma peak, in accordance with observations by Yang et al. (2013) from the same area, and similar to some southern Tian Shan samples (49–52, see also Liu et al., 2013).

4.6. MDS maps

MDS maps for each of the detrital zircon U–Pb age spectra, heavy mineral compositions, and bulk petrography show distinct grouping correlating with geographic sample origin (supplemental Fig. 1). As a further simplification, Fig. 3a contains an In-

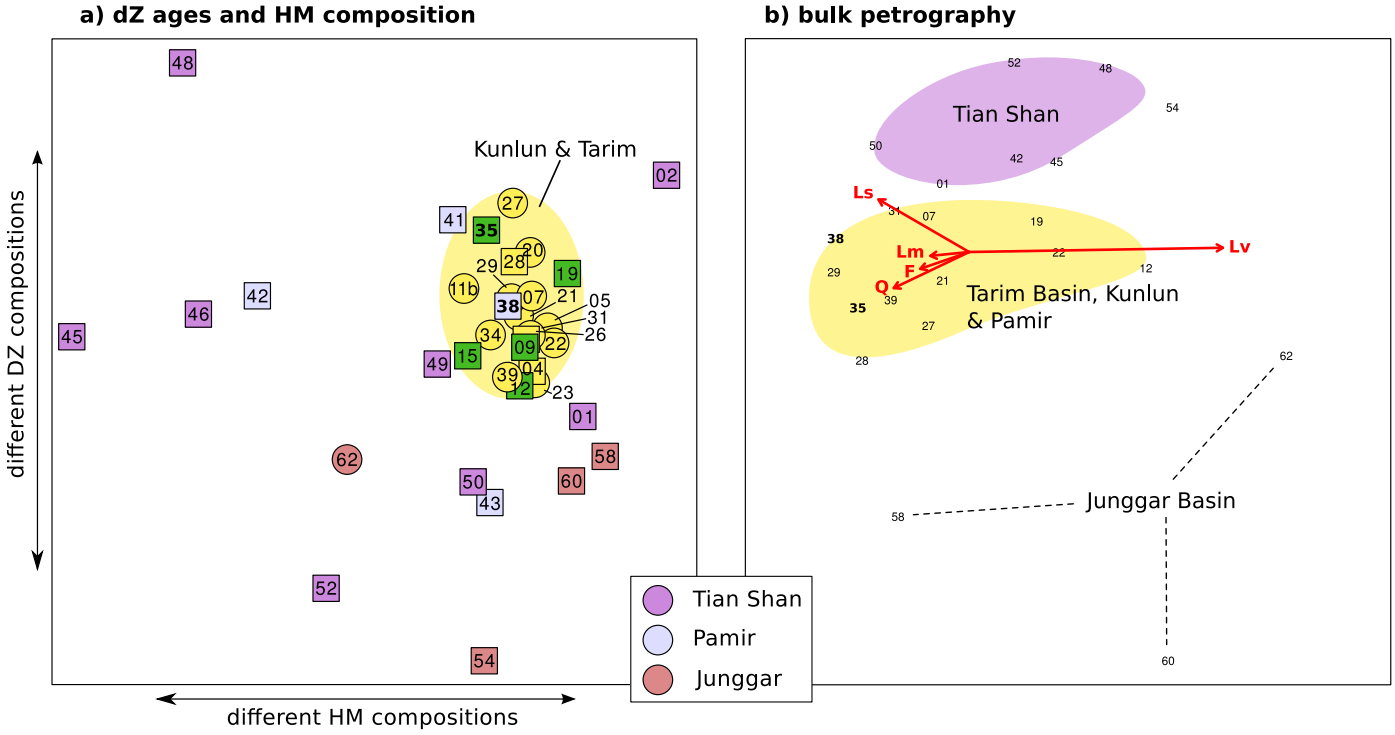

Fig. 3. a) INDSCAL map combining detrital zircon age spectra and heavy mineral compositions. NE-Pamir-derived samples overlap the Tarim – Kunlun field, except for the Kirzlsu river (42) and adjacent piedmont fan 43. b) PCA plot of bulk petrography. Tian Shan samples are characterised by a higher content of volcanic and sedimentary lithic components, Altai-influenced Junggar samples plot far outside the main cluster. Tian-Shan-derived sample 54, from the Junggar Basin, plots with the other samples from this mountain range. Hotan and Yarkan Rivers (35 and 38, respectively) highlighted.

dividual Differences Scaling map (INDSCAL; see Vermeesch and Garzanti, 2015) combining the detrital zircon age and heavy mineral datasets. The petrographic dataset was not included in this analysis due to a) its small size compared to the other two datasets, and b) the ability to plot the PCA loadings as a 'compositional biplot' showing influence of individual framework petrography components on plot position (Fig. 3b). The value of presenting the data in this way is to show which source areas have distinct signals, and which samples group together with the Tarim Basin–Taklamakan sands. These apparent relationships can then be verified by relating them back to the individual age spectra and compositional data. In other words, we use the MDS maps as a visual tool and to gain an indication of relationships, while final conclusions are based on the full data sets.

One major conceptual difference between 2-way MDS and INDSCAL is that, whereas the orientation of the 2-way MDS configuration is arbitrary (i.e. it can be rotated or reflected without loss of information), the orientation of a 3-way MDS configuration generally does have geological meaning. Because the 3-way MDS analysis in Fig. 3a comprises just two datasets, the dZ and HM datasets each apply completely different weights, so that the horizontal distribution of the data points is dominated by the HM distances and the vertical axis represents the dZ distances.

The PCA loadings of the petrographic data (Fig. 3b) show that a) most of the variability, and hence, most of the PT provenance information, is carried by the volcanic and sedimentary rock fragments and the quartz content (longest arrows), and b) there exists an anti-correlation between the proportions of volcanic and sedimentary rock fragments (arrows point in opposite directions), which is independent of the quartz component. In this plot, the Tian Shan can be clearly seen as characterised by a higher content of sedimentary and volcanic lithics than the bulk of the Tarim Basin and Kunlun Shan samples, whereas the (Altai-derived) Junggar Basin contains more volcanic lithics and quartz, without input from sedimentary sources.

5. Interpretation and discussion

Our goal is to understand the process of sediment transfer from source regions into the Tarim Basin and Taklamakan desert, to identify the main source regions, and then consider if the Tarim Basin could have been contributing to the sediments of the Chinese Loess Plateau (CLP). Based on the topography and hydraulic network detailed in section 2 and Fig. 1, the expectation would be that the basin fill would contain a significant amount of material eroded from the Tian Shan and NE Pamir. The bulk-petrography data suggest that the Yarkan River is a major source of the desert sediment. However, statistical visualisation of the multi-sample datasets and close inspection of the individual proxies reveals additional details of the routing system.

5.1. Junggar and Tian Shan sources

The multicomponent dataset allows us to compare signatures of potential source rocks and daughter sands of the Tarim Basin and Taklamakan dunes. On the compositional plots and MDS maps (Figs. 2 and 3), source regions that do not overlap with the Tarim Basin group, such as the Tian Shan, are unlikely to be major sources for the desert sands, unless they are mixing with other sources to result in the observed composition. The samples from the Junggar Basin–Altai range plot even more clearly outside of the main cluster of desert samples, suggesting no transfer of sand between the Junggar and Tarim Basin. It is conceivable that a mixture of Altai-derived and Tian-Shan derived material in the right proportions could result in a proxy signature as observed in the Tarim Basin. However, the Junggar Basin dune sample 62, which is located closest to the Tarim Basin and between the Altai and the Tian Shan, is distinctly dominated by volcanic lithics and shows the same age spectrum as the other Altai samples. This region can therefore be ruled out as a major sediment source for the Tarim Basin. Sources from the western margins of the basin, draining the

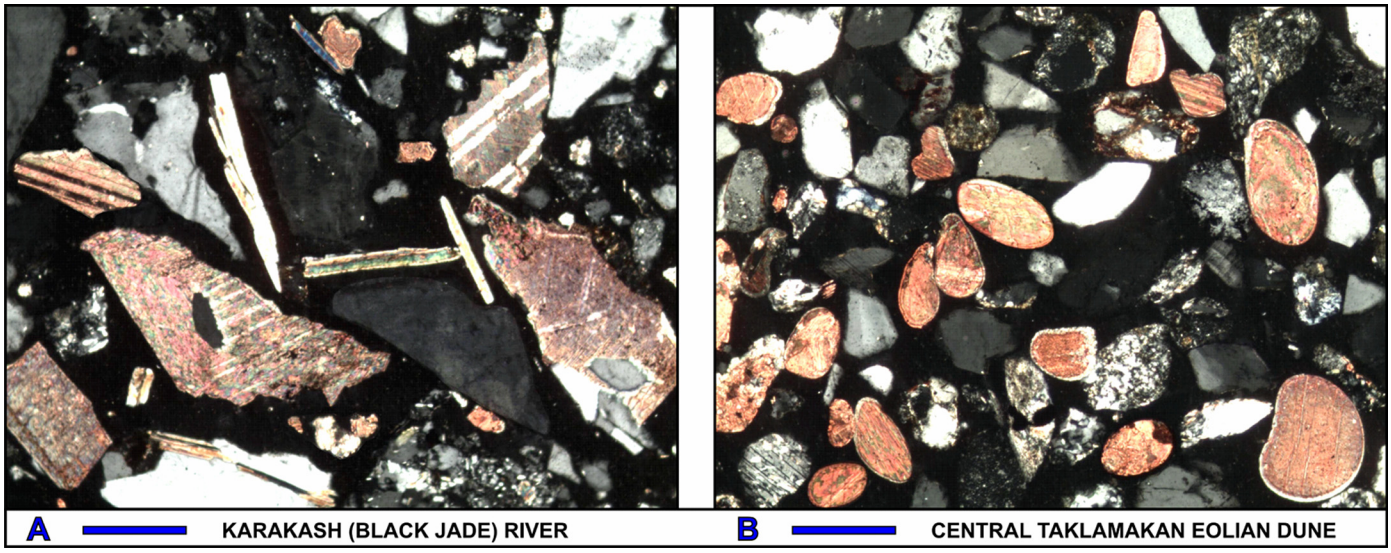

Fig. 4. Marked difference in grain roundness in fluvial (A; sample 35) and aeolian sands (B; sample 21). With their relatively low hardness, limestone rock fragments are easily rounded in the aeolian environment (Garzanti et al., 2015). They appear still angular in sand of the Karakash River draining the Kunlun mountains, but rounded to well rounded in the Taklamakan dune field. Photos with crossed polars; blue scale bars are 250 microns. Calcareous grains are stained with alizarine red to facilitate identification. (For interpretation of the references to colour in this figure legend, the reader is referred to the web version of this article.)

NE Pamir, mostly plot outside of the main cluster on the dZ plot, whereas they overlap in the PT map.

Based on its significance as a tributary to the main Tarim River, as mentioned in section 2, it is not surprising that out of the Tian Shan samples, the Aksu River (sample 50; with Toshkan sample 49) plots closest to the Tarim Basin group on the zircon and heavy mineral MDS map (Fig. 3) and in the compositional plots (Fig. 2). Within the Tarim Basin group, Tarim sample 26, taken downstream from the confluence with the Aksu, and dune samples 22 and 23, along an old or ephemeral path of the Tarim River in the northeast, plot nearest to the Aksu, indicating influence from this source. The Aksu signature is not seen in other desert samples from further south and west. Thus, despite the Tarim River draining most of the water leaving the Tian Shan, this mountain range does not appear to be a major source of the desert sands.

5.2. Kunlun/Altun Shan and Pamir sources

Rivers that drain the southern margin of the Tarim Basin, mainly the Kunlun Shan and Altun Shan, plot within the main cluster of Tarim–Taklamakan dune sands (Figs. 2 and 3), indicating that these areas might be key sources of the dune sand. As detailed in section 4.4, samples 27 and 28 trace the signature of the Karakash He through the basin, and thus plot near point 35 on the MDS map (Fig. 3). This affinity also shows in the petrographic and lithic components data (Fig. 2); in the latter, the Ls content decreases along the stream from sample 35, situated highest up along the river, via 29 down to 28 and 27 (see Fig. 1).

Compositional data seems to indicate that the Yarkan (sample 38) is the closest match to the Tarim Basin fill, indicating this river as the main sediment source. However, the Yarkan exhibits a characteristic young age peak at 120 Ma, also present in dune sample 39 close to the entry point into the basin, and traceable along the Tarim in samples 26, old river trunk 22 and 23, and to the most distal sample 07. This signature peak is missing from more central and southern dune samples 21, 20, 11b and even from sample 27, just south of the main Tarim trunk. This indicates that NE-to-SW aeolian mixing in the Taklamakan, for the grain sizes considered, is not pervasive over long distance.

Jointly considered, all three datasets show that sediments from the Taklamakan desert and rivers draining the Kunlun Mountains are very similar, especially for the dZ and HM datasets. In contrast, there exists considerable variability in the compositions of the Tian Shan, both between catchment areas and in comparison to the Tarim Basin, and distinct differences to the Junggar sands. This indicates that the Western Kunlun and Pamir are the dominant sources of Taklamakan desert sand.

5.3. Interplay of fluvial and aeolian transport

If rivers were the primary transporter of sand, then over time there should be very little sand left within the Tarim Basin as most of it would have been washed downstream into the Tarim main trunk and eastwards to its termination. The presence of abundant sand within the Taklamakan desert is testimony to wind removing sand from fluvial deposits and moving it within the basin at rates faster than the rivers can remove the sediment. Although a constant high sediment influx from the mountains in the south could also explain the presence of sand, these high sedimentation rates would be reflected in high accumulation rates either within the basin, or at the terminus of the Tarim River, which is not observed. On the other hand, if wind was the sole transport mechanism, all sand should accumulate in the southern part of the central basin where main wind directions converge, and strongly denudated plains similar to the Stony Gobi would be expected in the northeastern basin. So it appears that within the Tarim Basin, wind is a south-directed transport agent just strong enough to counteract the north-directed flow of water.

However, fluvial transport fluctuates over time and is not equally distributed across the basin, which can account for some of the variability amongst regions seen on the MDS maps. Figs. 2 and 3 show that the bulk of the Tarim–Taklamakan sands have provenance signatures diagnostic of Kunlun sources, thus any aeolian reworking appears more effective in the central and southern region of the basin, less so in the north. The foothills of the Kunlun contain extensive loess deposits reaching several km into the valleys, and recycling of these sediments into the rivers draining northwards could be expected. However, when comparing carbonate grains, which get rounded quickly in an aeolian environment (Garzanti et al., 2015), from Kunlun-derived river sands with Tarim Basin dune sands (Fig. 4), the river sediment shows very angular carbonate grains, without exhibiting the rounding seen in

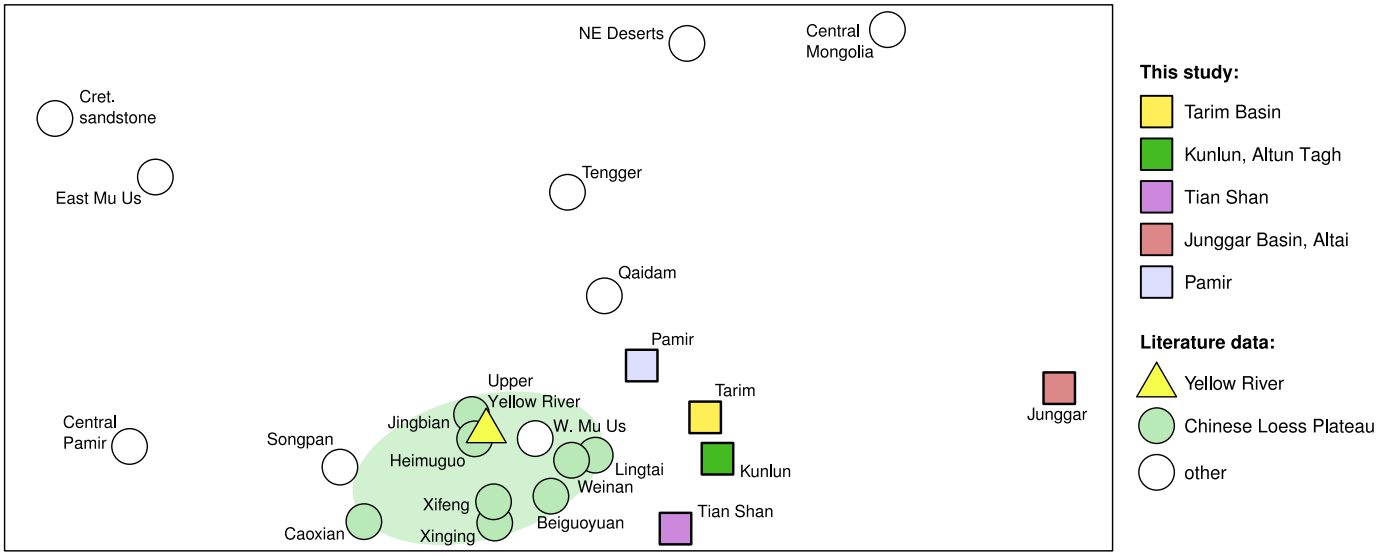

Fig. 5. Multidimensional Scaling Map based on calculated K–S distances between U–Pb age spectra, comparing modern sediment samples from the Chinese Loess Plateau (5768 ages) and possible source areas (5616 ages; both: Bird et al., 2015; Stevens et al., 2013; and references therein) with data from the upper reaches of the Yellow River (1265 ages; Nie et al., 2015) and this study (4047 ages).

the dune sands. Therefore, the similarity between Kunlun-derived river sources and the main Tarim Basin is not caused by mixing and recycling in the catchment areas, but by true similarity in provenance proxies, suggesting the Kunlun as a primary sediment source for the area. As the grain sizes analysed in this study did not include the finest dust fraction (few µm), a higher degree of regional homogenisation within smallest grain sizes cannot be entirely ruled out.

Aside from the Yarkan and Hotan Rivers, which connect to the Tarim River, most of the rivers that drain the Kunlun are ephemeral features that exist intermittently during flooding, and they usually terminate within the central basin without connecting to a larger trunk stream. As a consequence, this Kunlun-derived sediment is made available for reworking directly within the desert and does not need to be transported from far. Conversely, in the north of the basin, the west to east flowing Tarim River transports a large proportion of its sediment load away from the basin towards the eastern margin, where, near its terminus, it is deposited. With this, most of the sediment coming off the Tian Shan is removed in the wet season eastwards before it could reach the central desert, and Tian Shan sources are largely missing from the desert sands. The broad valley of the Tarim River, more humid and vegetated throughout the year, might contribute to this, forming a natural barrier against material blown out from the alluvial fans at the foot of the Tian Shan reaching the desert to the south.

5.4. *Implications for the provenance of the Chinese Loess Plateau*

The MDS maps, compositional data, and to a lesser degree the age spectra, clearly show that sand from the Altai and Junggar Basin has a different provenance signature from the Tarim Basin, thus we can rule out significant exchange of sand between these two basins. Given the distinct signatures of the Tarim Basin and Junggar Basin, it is possible to consider the wider question about how different these sands are from other Asian dust sources and the extent to which the Taklamakan might be a potential source of dust to the Loess Plateau. Fig. 5 is a summary MDS map based on dZ age spectra that compares potential sources for the Chinese Loess Plateau (16 696 individual grain ages; Stevens et al., 2013; Bird et al., 2015; Nie et al., 2015; and references therein) including the new data from this study. The Yellow River shows the closest affinity to the loess sediments (in orange), as well as to the western Mu Us desert. The Taklamakan samples are also fairly close to the loess, but the similarity in age spectra between the Kunlun/Tarim and the Yellow River/loess areas is most likely due to a common source region – the northern margin of the Tibet Plateau (Bird et al., 2015). Furthermore, in a detailed study of Yellow River sediment provenance, Nie et al. (2015) show that Chinese loess and the western Mu Us sands are dominantly formed from upper Yellow River sediment and that much of the river's upper reaches' sediment load is stored on the Chinese Loess Plateau. A direct transport, at least of coarse silt and fine sand, from the Tarim Basin to the Loess Plateau, and especially of coarser sand to the Mu Us desert, is unlikely, as the Qaidam Basin and the Tengger desert, both lying along the direct route from the Tarim Basin, show significantly different composition. This plot further illustrates the conclusion that the Altai/Junggar Basin (points 'Central Mongolia' and 'Junggar') can be ruled out as a source for the CLP.

6. Conclusions

The closed Tarim Basin has allowed us to study sediment routing processes in the interplay of wind and water transport, from source to sink. Visual inspection alone of the whole dataset (Fig. 1) would make drawing clear conclusions difficult, especially as differences between zircon age spectra and the mineralogical and petrographic datasets can be subtle. Pie charts are notoriously difficult to interpret (Tufte, 2001), and other forms of plotting (histograms, stacked bar charts) do not fare much better.

From the MDS/PCA maps, which help interpret the provenance proxies by clearly displaying groupings based on similarity, we conclude the following:

- Taklamakan dune sands are derived from southern and southwestern sources (Kunlun Shan, Karakorum, Altun Shan, and their hinterland on the Tibet Plateau and in the Pamir).
- Northern and northwestern sources from the Tian Shan can be clearly distinguished and contribute only small amounts of sediment to the desert.
- Taklamakan sands are very different from Junggar Basin sediments. Aeolian sediment transport between these two internally drained basins is insignificant.

In the case of the Tarim Basin, and for the very fine to coarse sand grain fractions sampled, our study has shown that fluvial transported sand is the dominant source. In some cases, long-distance fluvial transport can bypass the active sand desert (Hotan He), whereas aeolian processes are responsible for reworking and balancing the hydraulic transport in the opposite direction. Homogenisation of the finest grain size fractions that make up the dust load in large storm events, as suggested previously by Chen et al. (2007) and Yang et al. (2007), cannot be ruled out. Although similarities between the analysed sands from the Tarim Basin and sediment on the Chinese Loess Plateau exist, this is likely due to both areas sharing a common source area (the northern Tibet Plateau), rather than direct sediment transport from the Tarim Basin to the Chinese Loess Plateau (Nie et al., 2015).

The Tarim Basin has been intensively surveyed for hydrocarbon exploration. To evaluate the significance of our observations in relation to basin-wide sediment budgets and changes in flux throughout time, similar multi-proxy analyses should be undertaken on time slices of subsurface samples, when available. Future research should also consider different grain size fractions separately, to possibly further disentangle hydraulic from aeolian transport.

Acknowledgements

We would like to thank Fangying Zhu and Yingyong Chen, Nanjing University, China, for their help during fieldwork, and Chris Holdsworth and Randy Parrish, BGS NIGL, Keyworth, UK, for discussion and assistance in sample preparation and analysis. This study was supported by NERC Research Grant NE/I008837/1, NSFC grant No. 41321062, and ERC Starting Grant No. 259504. The manuscript has greatly benefited from review by A. Licht and one anonymous reviewer.

Appendix A. Supplementary material

Supplementary material related to this article can be found online at http://dx.doi.org/10.1016/j.epsl.2015.12.036.

References

Allen, M.B., Vincent, S.J., Wheeler, P.J., 1999. Late Cenozoic tectonics of the Kepingtage thrust zone: interactions of the Tien Shan and Tarim Basin, northwest China. Tectonics 18 (4), 639.

Amit, R., Enzel, Y., Mushkin, A., Gillespie, A., Batbaatar, J., Crouvi, O., Vandenberghe, J., An, Z., 2014. Linking coarse silt production in Asian sand deserts and quaternary accretion of the Chinese Loess Plateau. Geology 42 (1), 23–26.

Bird, A., Stevens, T., Rittner, M., Vermeesch, P., Carter, A., Andò, S., Garzanti, E., Lu, H., Nie, J., Zeng, L., Zhang, H., Xu, Z., 2015. Quaternary dust source variation across the Chinese Loess Plateau. Palaeogeogr. Palaeoclimatol. Palaeoecol. 435, 254–264.

Bosboom, R., Dupont-Nivet, G., Grothe, A., Brinkhuis, H., Villa, G., Mandic, O., Stoica, M., Huang, W., Yang, W., Guo, Z., Krijgsman, W., 2014. Linking Tarim Basin sea retreat (west China) and Asian aridification in the late Eocene. Basin Res. 26 (5), 621–640.

Bullard, J.E., McTainsh, G.H., 2003. Aeolian–fluvial interactions in dryland environments: examples, concepts and Australia case study. Prog. Phys. Geogr. 27 (4), 471–501.

Carroll, A.R., Dumitru, T.A., Graham, S.A., Hendrix, M.S., 2013. An 800 million-year detrital zircon record of continental amalgamation: Tarim basin, NW China. Int. Geol. Rev. 55 (7), 818–829.

Chen, J., Li, G., Yang, J., Rao, W., Lu, H., Balsam, W., Sun, Y., Ji, J., 2007. Nd and Sr isotopic characteristics of Chinese deserts: implications for the provenances of Asian dust. Geochim. Cosmochim. Acta 71 (15), 3904–3914.

Chen, Y., Takeuchi, K., Xu, C., Chen, Y., Xu, Z., 2006. Regional climate change and its effects on river runoff in the Tarim Basin, China. Hydrol. Process. 20 (10), 2207–2216.

Coutand, I., Strecker, M.R., Arrowsmith, J.R., Hilley, G., Thiede, R.C., Korjenkov, A., Omuraliev, M., 2002. Late Cenozoic tectonic development of the intramontane Alai Valley (Pamir–Tien Shan region, central Asia): an example of intracontinental deformation due to the Indo-Eurasia collision. Tectonics 21 (6) 3-1–3-19.

Cowgill, E., 2010. Cenozoic right-slip faulting along the eastern margin of the Pamir salient, northwestern China. Bull. Geol. Soc. Am. 122 (1–2), 145–161.

Cowgill, E., Yin, A., Harrison, T.M., Xiao-Feng, W., 2003. Reconstruction of the Altyn Tagh fault based on U–Pb geochronology: role of back thrusts, mantle sutures, and heterogeneous crustal strength in forming the Tibetan Plateau. J. Geophys. Res., Solid Earth 108 (B7).

Crouvi, O., Amit, R., Enzel, Y., Gillespie, A.R., 2010. Active sand seas and the formation of desert loess. Quat. Sci. Rev. 29 (17–18), 2087–2098.

Dai, J., Wang, C., Hourigan, J., Santosh, M., 2013. Multi-stage tectono-magmatic events of the Eastern Kunlun Range, northern Tibet: insights from U–Pb geochronology and (U–Th)/He thermochronology. Tectonophysics 599, 97–106.

Dong, Z., Wang, X., Chen, G., 2000. Monitoring sand dune advance in the Taklimakan Desert. Geomorphology 35 (3–4), 219–231.

Dumitru, T.A., Zhou, D., Chang, E.Z., Graham, S.A., Hendrix, M.S., Sobel, E.R., Carroll, A.R., 2001. Uplift, exhumation, and deformation in the Chinese Tian Shan. Mem. Geol. Soc. Amer. 194, 71–99.

Field, J.P., Breshears, D.D., Whicker, J.J., 2009. Toward a more holistic perspective of soil erosion: why aeolian research needs to explicitly consider fluvial processes and interactions. Aeolian Res. 1 (1–2), 9–17.

Garzanti, E., Resentini, A., Andò, S., Vezzoli, G., Pereira, A., Vermeesch, P., 2015. Physical controls on sand composition and relative durability of detrital minerals during ultra-long distance littoral and aeolian transport (Namibia and southern Angola). Sedimentology 62, 971–996.

Ge, R., Zhu, W., Wilde, S.A., He, J., Cui, X., Wang, X., Bihai, Z., 2014. Neoproterozoic to Paleozoic long-lived accretionary orogeny in the northern Tarim Craton. Tectonics 33 (3), 302–329.

Gehrels, G., Kapp, P., Decelles, P., Pullen, A., Blakey, R., Weislogel, A., Ding, L., Guynn, J., Martin, A., McQuarrie, N., Yin, A., 2011. Detrital zircon geochronology of pre-Tertiary strata in the Tibetan–Himalayan orogen. Tectonics 30 (5).

Gehrels, G.E., Yin, A., Wang, X.-F., 2003. Detrital-zircon geochronology of the northeastern Tibetan plateau. Geol. Soc. Am. Bull. 115 (7), 881–896.

Huang, J., Wang, T., Wang, W., Li, Z., Yan, H., 2014. Climate effects of dust aerosols over East Asian arid and semiarid regions. J. Geophys. Res., Atmos. 119 (19), 11,398–11,416.

Jarvis, A., Reuter, H.I., Nelson, A., Guevara, E., 2008. Hole-filled SRTM for the globe version 4. Available from the CGIAR-CSI SRTM 90 m database, //srtm.csi.cgiar.org.

Jiang, X., 2004. Lithospheric deformation beneath the Altyn Tagh and West Kunlun faults from recent gravity surveys. J. Geophys. Res. 109 (B5), B05406.

Kao, H., Gao, R., Rau, R.J., Shi, D., Chen, R.Y., Guan, Y., Wu, F.T., 2001. Seismic image of the Tarim basin and its collision with Tibet. Geology 29 (7), 575–578.

Knippertz, P., Stuut, J.-B.W. (Eds.), 2014. Mineral Dust. Springer, Netherlands, Dordrecht.

Kundzewicz, Z.W., Merz, B., Vorogushyn, S., Hartmann, H., Duethmann, D., Wortmann, M., Huang, S., Su, B., Jiang, T., Krysanova, V., 2015. Analysis of changes in climate and river discharge with focus on seasonal runoff predictability in the Aksu River Basin. Environ. Earth Sci. 73 (2), 501–516.

Liu, D., Jolivet, M., Yang, W., Zhang, Z., Cheng, F., Zhu, B., Guo, Z., 2013. Latest Paleozoic–Early Mesozoic basin–range interactions in South Tian Shan (northwest China) and their tectonic significance: constraints from detrital zircon U–Pb ages. Tectonophysics 599, 197–213.

Liu, J., Zheng, Y., Li, Z., Flynn, C., Welton, E.J., Cribb, M., 2011. Transport, vertical structure and radiative properties of dust events in southeast China determined from ground and space sensors. Atmos. Environ. 45 (35), 6469–6480.

Nie, J., Stevens, T., Rittner, M., Stöckli, D.F., Garzanti, E., Limonata, M., Bird, A., Andò, S., Vermeesch, P., Saylor, J., Lu, H., Breecker, D., Hu, X., Liu, S., Resentini, A., Vezzoli, G., Peng, W., Carter, A., Ji, S., Pan, B., 2015. Loess Plateau storage of Northeastern Tibetan Plateau derived Yellow River sediment. Nat. Commun. 6 (8511).

Roger, F., 2003. Geochronological and geochemical constraints on Mesozoic suturing in east central Tibet. Tectonics 22 (4).

Seltmann, R., Konopelko, D., Biske, G., Divaev, F., Sergeev, S., 2011. Hercynian post-collisional magmatism in the context of Paleozoic magmatic evolution of the Tien Shan orogenic belt. J. Asian Earth Sci. 42 (5), 821–838.

Shu, L.S., Deng, X.L., Zhu, W.B., Ma, D.S., Xiao, W.J., 2011. Precambrian tectonic evolution of the Tarim Block, NW China: new geochronological insights from the Quruqtagh domain. J. Asian Earth Sci. 42 (5), 774–790.

Smith, B.J., Wright, J.S., Whalley, W.B., 2002. Sources of non-glacial, loess-size quartz silt and the origins of "desert loess". Earth-Sci. Rev. 59 (1–4), 1–26.

Sobel, E.R., 1999. Basin analysis of the Jurassic–Lower Cretaceous southwest Tarim basin, northwest China. Geol. Soc. Am. Bull. 111 (5), 709–724.

Stevens, T., Carter, A., Watson, T.P., Vermeesch, P., Andò, S., Bird, A.A.F., Lu, H., Garzanti, E., Cottam, M.A., Sevastjanova, I., 2013. Genetic linkage between the Yellow River, the Mu Us desert and the Chinese Loess Plateau. Quat. Sci. Rev. 78, 355–368.

Sun, J., 2002. Source regions and formation of the loess sediments on the high mountain regions of northwestern China. Quat. Res. 58 (3), 341–351.

Sun, J., Liu, T., 2006. The age of the Taklimakan Desert. Science (New York) 312 (5780), 1621.

Svensson, A., Biscaye, P.E., Grousset, F.E., 2000. Characterization of late glacial continental dust in the Greenland Ice Core Project ice core. J. Geophys. Res. 105 (D4), 4637.
Tsuchiya, K., Oguro, Y., 2007. Observation of large fixed sand dunes of Taklimakan Desert using satellite imagery. Adv. Space Res. 39 (1), 60–64.
Tufte, E.R., 2001. The Visual Display of Quantitative Information. Graphics Press.
Vermeesch, P., 2012. On the visualisation of detrital age distributions. Chem. Geol. 312–313, 190–194.
Vermeesch, P., 2013. Multi-sample comparison of detrital age distributions. Chem. Geol. 341, 140–146.
Vermeesch, P., Garzanti, E., 2015. Making geological sense of 'Big Data' in sedimentary provenance analysis. Chem. Geol. 409, 20–27.
Wang, X., Dong, Z., Zhang, J., Chen, G., 2002. Geomorphology of sand dunes in the Northeast Taklimakan Desert. Geomorphology 42 (3–4), 183–195.
Xiao, W., Windley, B.F., Allen, M.B., Han, C., 2013. Paleozoic multiple accretionary and collisional tectonics of the Chinese Tianshan orogenic collage. Gondwana Res. 23 (4), 1316–1341.
Xiao, W.J., Windley, B.F., Liu, D.Y., Jian, P., Liu, C.Z., Yuan, C., Sun, M., 2005. Accretionary tectonics of the Western Kunlun Orogen, China: a Paleozoic–Early Mesozoic, long-lived active continental margin with implications for the growth of Southern Eurasia. J. Geol. 113 (6), 687–705.
Xie, J., Wu, F.T., Ding, Z.L., 2007. Detrital zircon composition of U–Pb ages and Hf isotope of the Hunshandake sandy land and implications for its provenance. Acta Petrol. Sin. 23 (2), 523–528.
Xu, B., Jian, P., Zheng, H., Zou, H., Zhang, L., Liu, D., 2005. U–Pb zircon geochronology and geochemistry of Neoproterozoic volcanic rocks in the Tarim Block of northwest China: implications for the breakup of Rodinia supercontinent and Neoproterozoic glaciations. Precambrian Res. 136 (2), 107–123.
Xu, Z., Lu, H., Zhao, C., Wang, X., Su, Z., Wang, Z., Liu, H., Wang, L., Lu, Q., 2011. Composition, origin and weathering process of surface sediment in Kumtagh Desert, Northwest China. J. Geogr. Sci. 21 (6), 1062–1076.
Yang, W., Jolivet, M., Dupont-Nivet, G., Guo, Z., Zhang, Z., Wu, C., 2013. Source to sink relations between the Tian Shan and Junggar Basin (northwest China) from Late Palaeozoic to Quaternary: evidence from detrital U–Pb zircon geochronology. Basin Res. 25 (2), 219–240.
Yang, X., Zhu, B., White, P.D., 2007. Provenance of aeolian sediment in the Taklamakan Desert of western China, inferred from REE and major-elemental data. Quat. Int. 175 (1), 71–85.
Yang, Y., 2002. Cenozoic deformation of the Tarim plate and the implications for mountain building in the Tibetan Plateau and the Tian Shan. Tectonics 21 (6), 1–17.
Ye, Z., Chen, Y., Zhang, X., 2014. Dynamics of runoff, river sediments and climate change in the upper reaches of the Tarim River, China. Quat. Int. 336, 13–19.
Yin, A., Harrison, T.M., 2000. Geologic evolution of the Himalayan–Tibetan orogen. Annu. Rev. Earth Planet. Sci. 28 (1), 211–280.
Yumimoto, K., Eguchi, K., Uno, I., Takemura, T., Liu, Z., Shimizu, A., Sugimoto, N., 2009. An elevated large-scale dust veil from the Taklimakan Desert: intercontinental transport and three-dimensional structure as captured by CALIPSO and regional and global models. Atmos. Chem. Phys. 9 (21), 8545–8558.
Zhang, C.-L., Zou, H.-B., Li, H.-K., Wang, H.-Y., 2013. Tectonic framework and evolution of the Tarim Block in NW China. Gondwana Res. 23 (4), 1306–1315.
Zhang, C.-L.L., Li, Z.-X.X., Li, X.-H.H., Ye, H.-M.M., 2009. Neoproterozoic mafic dyke swarms at the northern margin of the Tarim Block, NW China: age, geochemistry, petrogenesis and tectonic implications. J. Asian Earth Sci. 35 (2), 167–179.
Zhang, Z., Wang, H., Guo, Z., Jiang, D., 2007. What triggers the transition of palaeoenvironmental patterns in China, the Tibetan Plateau uplift or the Paratethys Sea retreat? Palaeogeogr. Palaeoclimatol. Palaeoecol. 245 (3–4), 317–331.
Zheng, H., Wei, X., Tada, R., Clift, P.D., Wang, B., Jourdan, F., Wang, P., 2015. Late oligocene–early miocene birth of the Taklimakan Desert. Proc. Natl. Acad. Sci. USA 112 (25), 7662–7667.